CYTOMETRY
Journal of Quantitative Cell Science PART A

Nanoliposomes Co-Encapsulating Photoswitchable Probe and Photosensitizer for Super-Resolution Optical Imaging and Photodynamic Therapy

Hao Xu,[#] Bingling Chen,[#] Wanjun Gong,[#] Zhigang Yang, Junle Qu[*]

Key Laboratory of Optoelectronic Devices and Systems of Ministry of Education and Guangdong Province, College of Physics and Optoelectronic Engineering, Shenzhen University, Shenzhen, Guangdong Province, 518060 China

Received 26 April 2019; Revised 28 May 2019; Accepted 1 July 2019

Grant sponsor: (Key) Project of Department of Education of Guangdong Province, Grant number: 2015KGJHZ002, Grant number: 2016KCXTD007; Grant sponsor: Guangdong Natural Science Foundation Innovation Team, Grant number: 2014A030312008, Grant number: 2017A030310136; Grant sponsor: National Natural Science Foundation of China, Grant number: 61525503, Grant number: 61620106016, Grant number: 61705139, Grant number: 61835009, Grant number: 61875135, Grant number: 81727804; Grant sponsor: Shenzhen Basic Research Project, Grant number: JCYJ20150930104948169, Grant number: JCYJ20160328144746940, Grant number: JCYJ20170412105003520, Grant number: JCYJ20170817094735945, Grant number: JCYJ20170818090620324

Additional Supporting Information may be found in the online version of this article.

[*]Correspondence to: Junle Qu, Key Laboratory of Optoelectronic Devices and Systems of Ministry of Education and Guangdong Province College of Physics and Optoelectronic Engineering, Shenzhen University Shenzhen, Guangdong Province 518060, China
Email: jlqu@szu.edu.cn

[#]These authors contributed equally to the work.

Published online in Wiley Online Library (wileyonlinelibrary.com)

DOI: 10.1002/cyto.a.23864

Abstract

Photosensitizers (PSs) are ideal cancer theranostic drugs that can be administered as both fluorescence imaging reagents and photodynamic therapy (PDT) drugs. To improve the tumoritropic behavior of PSs, nanoliposomes are presently being considered as optimal PSs carriers. Although nanoliposomal PSs have been utilized in clinical therapy, PSs localization and photosensitive processing in nanoliposomal PSs are rarely observed on nanoscale. Investigating changes in the fine structure of nanoliposomes under photosensitive processing will further our understanding of the photosensitive effect on nanoliposomal PSs. In this study, nanoliposomes co-encapsulating the PSs benzoporphyrin derivative monoacid A (BPD) and the photoswitchable probe Cy5-927 were prepared to realize PDT and nanoscale super-resolution optical imaging. The fine structures of nanoliposomal BPD and Cy5-927 (LBC) were visualized by a home-built stochastic optical reconstruction microscopy (STORM). Our PDT results showed that the photorelease and PDT efficiency of BPD were not decreased by co-encapsulating with Cy5-927 in LBC. Taken together, LBC can be used as a new optical probe and PDT reagent for investigating changes in nanoliposomes fine structure and micro-interaction in the cellular process of PDT. Therefore, our results deepened our understanding of liposome-based PDT for optimizing cancer treatment.

Key terms

nanoliposome; photodynamic therapy; photosensitizer; photoswitchable probe; super-resolution optical imaging

Photodynamic therapy (PDT) is a photochemical modality involving activation of nontoxic photosensitizers (PSs) using a harmless light (wavelength specific) to generate cytotoxic reactive molecular species that kill or modulate target cells and tissues. PDT, compared to other therapies (e.g., chemotherapy and radiation), allows localization of both light and PSs at target sites to achieve more precise, spatiotemporally controlled therapeutic actions (1). Especially, hydrophobic PSs can directly kill tumor cells by penetrating deeply into them to disintegrate their membranes and organelles (2). However, the water insolubility of hydrophobic compounds needs to be overcome in the pharmacy.

The motivated development of nanotechnology for drug delivery in oncologic applications has led to various new therapeutic approaches, including delivery of PSs for PDT (3–5), which can be used to optimize hydrophobic PSs for utilization in cancer therapy. To date, Visudyne®, a liposomal benzoporphyrin derivative monoacid A (BPD) formulation, is the FDA-approved photonanomedicine for PDT of age-related macular degeneration. (3). The clinical impact of BPD is further evidenced in ongoing clinical trials (6,7). In addition to improving the solubility and pharmacokinetics of PSs, liposomal nanotechnology offers a unique opportunity to

co-package multiple PSs and/or drugs, thereby unifying their pharmacokinetics to maintain their ratio until arrival at a tumor site (8,9). Moreover, the liposomal membrane can provide sufficient sites for conjugation with multiple functional ligands; thus, nanoliposomes with a specifically modified surface have been designed for enhanced pharmacokinetic properties as well as improved therapeutics (10). Currently, He et al. have developed multiagent nanoparticles to deliver cisplatin and the PSs pyropheophorbide for combined chemotherapy and PDT. They also found that releasing the two reagents in a triggered manner could synergistically induce cancer cell apoptosis and necrosis (11). Besides, Hasan's group has also demonstrated that the optimal incorporation of insoluble BPD into the lipid bilayer can enhance photocytotoxicity (9), reduce drug efflux from cells (8), and realize spatiotemporal control of drug photorelease (12).

Although the efficacy of PDT and safety of PSs can be substantially improved by using liposomal formulations (13), the micro-mechanisms of the interaction of nanoliposomes with cells and its photorelease in PDT remain to be further investigated. Especially, extensively used nanoliposomes, with size smaller than 200 nm, showed enhanced passive tumor uptake through the enhanced permeability and retention (EPR) effect because their small size allows entrance to the tumor vasculature (14). However, these small-sized liposomes are difficult to be visualized by conventional optical imaging methods because the optical diffraction limit defines the spatial resolution. Although the morphology of nanoliposomes can be observed by some conventional imaging methods, such as transmission electronic microscopy (TEM), scanning electronic microscopy (SEM), or atomic force microscopy (AFM), these methods are time-consuming because they always require dry liposomes and invasive, high-vacuum environment (15). Currently, super-resolution fluorescent microscopy is available as a new method to directly observe the fine nanostructures of nanoliposomes, with the amphiphilic photoswitchable fluorophore as a staining agent (16). Therefore, choosing the optimal photoswitchable fluorophore to combine with liposomal PSs is important for investigating liposomal PSs in PDT.

As one of the oldest and most investigated organic fluorophore family, the cyanine dyes' history could trace back to nearly 160 years ago when a fluorescent solid was synthesized by Williams. From that time on, the cyanine dyes are widely used as photosensors in varied applications (17–19). Because of its remarkable photophysical properties, fluorescence efficiencies, and wide-range of fluorescence, these species were developed at excellent fluorescent probes for bio-imaging. Moreover, with the increasing interest in single-molecule-based spectroscopy, the polymethine compounds become the fluorophores of choice for single-molecular Forster resonance energy Transfer (sm-FRET). In the last decades, several fluorescence microscopy technologies have broken the diffraction limitation and gained tremendous attentions. Among the three major super-resolution microscopy techniques, the stochastic optical reconstruction microscopy (STORM) offers new approach to observe the structure and interaction of subcellular organelles with a spatial resolution virtually at the molecular level (20,21). Although a few organic fluorescent molecules were found to be useful in STORM (22), the first and most commonly used probes—cyanine dyes—are still of much significance due to their spontaneous "blinking," which is an essential elements required for STORM.

In our research, in order to perform super-resolution imaging, a typical indodicarbocyanine dyes Cy5 was chosen. By inducing a phenyl group on one side of the indole, the hydrophobicity of the probe was increased. Moreover, a 1, 3, 2-dithiarsenolane moiety was modified on the other side of indole to synthesize the new fluorescent arsenicals called Cy5-927 (the relative molecular mass is 927). The arsenicals moiety can selectively bind to vicinal dithiol proteins (VDPs) by forming covalent bonds (23). Mitochondria possess abundant VDPs, which play essential roles in maintaining mitochondrial redox homeostasis, antioxidant defense, and redox signaling. Therefore, Cy5-927 can be considered as a biomolecular target to visualize the ultra-fine mitochondrial structures by super-resolution optical imaging.

In the current study, we performed super-resolution imaging and PDT by co-delivery of Cy5-927 and BPD via nanoliposomes to achieve synchronous pharmacokinetics. Potentially, this strategy could be used to visualize the fine nanostructures of liposome and optimize the PDT efficiency of liposomal PSs. The characteristics of LBC were examined, including their particle size, zeta potential, stability, and photorelease. The fine structure of LBC was observed by STORM imaging. Furthermore, the *in vitro* PDT therapeutic efficacy of LBC was compared with that of free BPD and liposomal BPD (LB) in HeLa cells. The results showed that the photodynamic cytotoxicity of BPD did not decrease following co-encapsulation with Cy5-927 in LBC.

Materials and Methods

Synthesis of LBC

Lipid compositions of 1,2-dipalmitoylsn-glycero-3-phosphocholine (DPPC), 1,2-dioleoyl-3-trimethylammonium-propane (chloride salt) (DOTAP), 1,2-distearoyl-sn-glycero-3-phosphoethanolamineN-[amino(polyethylene, glycol)-2000] (ammonium salt) (DSPE-PEG2000) and cholesterol (Avanti Polar Lipids Inc, Alabaster, AL) were mixed in chloroform at a molar ratio of 10:1:1:5. BPD (U.S. Pharmacopeial Convention, Rockville, MD) solution (50 mM in acetone) and Cy5-927 (synthesized by our laboratory) solution (50 mM in acetone) were mixed with the lipid mixture in a glass flask, and the organic solvents were evaporated using a rotary evaporation system to make a thin lipid film. The Cy5-927 and BPD-containing lipid film were hydrated in phosphate buffered saline (PBS). The hydrated solution was then subjected to 10 freeze–thaw cycles (4–45°C). The dispersions were extruded through polycarbonate membranes (200 nm pore size, Avanti Polar Lipids Inc, Alabaster, AL) at 42°C to form unilamellar vesicles. Unencapsulated agents were removed by dialysis overnight against PBS at 4°C using a 300 KD Spectra/Por® Float-A-Lyzer® G2 system (Spectrum® Laboratories, Rancho Dominguez, CA). BPD in nanoliposomes (LB) or Cy5-927 in

nanoliposomes (LC) were also prepared separately using the aforementioned method.

Characterization of LBC

The size, polydispersity index (PDI), and zeta potential of nanoliposomes were measured by dynamic light scattering using a Zetasizer Nano ZS90 (Malvern Instruments, Malvern, UK). The absorbance spectra of LB, LC, and LBC in Dimethyl Sulfoxide (DMSO) were measured by a spectrophotometer (LAMBDA 750 UV/VIS/NIR, PerkinElmer). The molar extinction coefficients (MECs) of BPD at 435 nm and Cy5-927 at 650 nm were determined, respectively, by calculating the slope of the concentration and absorbance standard lines of BPD and Cy5-927 at corresponding wavelength. The concentration of BPD and Cy5-927 in liposomal PSs was determined according to their MEC. The PSs leaking out of the stored nanoliposomes were monitored by dialyzing free PSs in the 300 KD dialysis system at different time intervals. The residual concentration of PSs inside the nanoliposomes was determined by measuring their absorbance spectrum after the dialysis. The leakage of PSs from nanoliposomes was calculated by subtracting the residual concentration from the original concentration. The drug photorelease was also investigated with the same method. Dark release ratio (no irradiation with laser) and photoinduced drug release ratio (irradiation with 690 nm laser) were measured using dialysis system in PBS at 37°C with 10% fetal bovine serum.

Super-Resolution Optical Imaging of LBC

LBC suspension was dropped onto a clean coverslip and dried. The raw image was obtained using a home-built system consisting of an Olympus IX 81 inverted optical microscope equipped with a high-numerical-aperture (NA) oil-immersion objective (100× UPlanSApo, NA 1.4; Olympus), a 656 nm solid-state laser (460 mW; CNI Laser China), and an EMCCD camera (iXon Ultra 897; Andor). Electronic shutters equipped with neutral density filters (Optical Densities from 0.1 to 4.0, THORLABS) were used to control the laser irradiance and a custom filter set (LED-DA/FI/TR/Cy5-4X4M-B-000; Semrock) was used to separate the emission from scattering laser and impurity fluorescence. The laser beam was guided into the microscope for direct activation of the sample with maximal illuminating intensity of 1.54 kW cm^{-2}. The Cy5-927 red dyes automatically switch into blinking state under such high intensity irradiation. An open source package written in python was used for the acquisition of STORM raw data (http://zhuang.harvard.edu/). Images were recorded typically at 60 Hz for 256×256 pixels (~160 nm per pixel). ImageJ plugin written in Java was used to analyze the image.

Cell Culture and in vitro PDT

HeLa cells were maintained in complete Dulbecco's Modified Eagle Medium (DMEM) (contained 1% (v/v) 5,000 I.U. per mL penicillin/streptomycin and 10% (v/v) fetal bovine serum) at 37°C in a 5% CO_2 incubator. Before PDT, HeLa cells (50,000 cells per well) were seeded in 35 mm cell culture treated plates and maintained at 37°C in a 5% CO_2 incubator. After 24 h, attached cells were incubated with free PSs or LPSs according to experimental concentration in culture media for 90 min under subdued light conditions. And then, all the cells were washed and replenished with 2 ml of fresh culture media and exposed to a laser irradiation system immediately. In this system, light was delivered from a 690 nm fiber-coupled diode laser (MRL-III-690; Changchun New Industries Optoelectronics Technology Co. Changchun, China) which was connected to the optical fiber and the laser power density was adjusted to 50 mW/cm^2. Dark toxicity of PSs and control groups were prepared in the same manner without laser irradiation. All the dishes were then incubated 24 h at 37°C under 5% CO_2. Next day, cell survival rates were assessed using commercial CCK-8 cell viability test. CCK-8 kits (Dojindo, Japan) containing a water-soluble tetrazolium salt (WST-8) can be reduced to a yellow-colored formazan dye by dehydrogenase activities (24). All cell culture plates were washed and replenished with 1 ml complete cell culture medium containing 100 µl CCK-8 solution. Threefold replicates were run and the absorbance at 450 nm of all the groups were measured by a multimode microplate reader (Spark®, Tecan). All experiments were repeated at least three times.

Data Analysis

All experiments were performed in triplicate and the data were expressed as mean plus and minus the standard deviation. T-test was used to determine the statistically significant differences among different groups when appropriate.

Results

Physical Characterization of LBC

LBC was fabricated by encapsulating both BPD and Cy5-927 in the sterically stabilized moderately cationic PEGylated liposomes made with DPPC, DOTAP, DSPE-PEG2000 and cholesterol. BPD and Cy5-927 are entrapped in the lipid bilayer (Fig. 1). The nanoliposome that contained only BPD (LB) or Cy5-927 (LC) was also prepared with the same phospholipid composition for the control experiments.

The characteristics of these prepared nanoliposome are listed in Table 1. The average diameter of the LBC was ~188.3 nm, similar to the size of LB and LC, indicating that the Cy5-927 co-encapsulation with BPD did not modify the nanoliposome size (25). The nanoliposome in our study was slightly cationic (Table. 1) due to the DOTAP in the lipid composition.

The absorbance spectra of LBC, LB, and LC in DMSO are shown in Figure 2a. LB has a strong absorbance peak at 689 nm (Fig. 2a green line) while LC has absorbance maximum at 662 nm (Fig. 2a, red line). The optical absorption of LBC (Fig. 2a, blue line) has multiple absorbance peaks representative of the BPD and Cy5-927 presence. Their fluorescence spectra have been measured with excitation wavelength of 435 nm and 656 nm, respectively (Fig. 2b). LBC and LB have significant fluorescence peaks close to 695 nm at 435 nm excitation. However, LC has very low fluorescence signal at 435 nm excitation. In contrast, LBC and LC have significant fluorescence intensity close to 671 nm at 656 nm excitation. Meanwhile, LB has very low fluorescence intensity at 656 nm excitation, which indicated that BPD has very low fluorescence signal when BPD

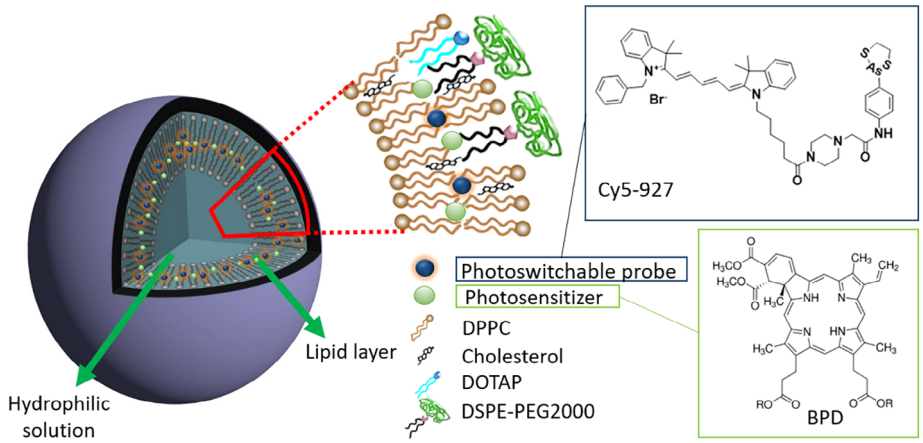

Figure 1. The schematic diagram of NL-co-encapsulated BPD and Cy5-927 (LBC) with the BPD and Cy5-927 in the bilayer of liposome. [Color figure can be viewed at wileyonlinelibrary.com]

and Cy5-927 were excited at 656 nm at the same time. Therefore, BPD has less influence on the Cy5-927 fluorescence signal when LBC was excited at 656 nm laser irradiation.

The concentration of BPD and Cy5-927 in the LBC can be calculated using the standard absorbance curve of BPD or Cy5-927 in DMSO according to the following equations:

$$C_B = \frac{A_{435}}{M_{B435}} \quad (1)$$

$$C_c = \frac{A_{650} - C_B \times M_{B650}}{M_{c650}} \quad (2)$$

where C_B and C_c stand for the concentration of BPD and Cy5-927. A_{435} and A_{650} represent the absorbance of the LBC at 435 nm and 650 nm, respectively. M_{B435}, M_{B650}, and M_{C650} indicate the MECs of BPD and Cy5-927 at 435 nm or 650 nm.

The PSs loading efficiency in LBC and control nanoliposomes was calculated as a percentage of the concentration of regents in the nanoliposomes to the initial concentration of regents used to prepare the nanoliposomes. The results are shown in Table 1. The loading efficiency of Cy5-927 in the LBC and LC was about 51.1% and 57.5%, respectively. The BPD loading efficiency in LBC and LB was 71.2% and 80.9%, respectively. The similar loading efficiencies observed between LB and LBC indicated that the BPD did not interfere with the encapsulation of Cy5-927 into the hydrophobic lipid film during the extrusion process.

Table 1. The particle size, zeta-potential, and the PSs loading percentage in NL (LB), Cy5-927 in NL (LC) and NL-co-encapsulated BPD and Cy5-927 (LBC)

NL	SIZE (NM)	ZETA POTENTIAL (MV)	BPD LOADING (%)	CY5-927 LOADING (%)
LBC	188.3 ± 0.7	5.1 ± 0.3	71.2 ± 4.8	51.1 ± 6.2
LB	179.5 ± 0.8	6.5 ± 0.9	80.9 ± 2.1	N/A
LC	182.4 ± 0.4	4.7 ± 0.8	N/A	63.5 ± 5.3

We compared the leakage of the PSs from the LBC and the control liposomes (Fig. 3a). The leakage of BPD or Cy5-927 was <5% in LB, LC, or LBC for a 10 day storage period. The BPD and Cy5-927 leakage were not significantly different in LBC from the control liposomes until Day 30. The difference between the LBC and control liposomes was observed only at later time points. Furthermore, no statistically significant change was observed in the size and zeta potential of the liposomes (LBC, LB and LC) during 40 days of storage at 4 °C, indicating the intact stability of the liposomes. The PDI of the liposomes was also lower than 0.1, indicating the absence of aggregation during this storage period (Supporting Information Fig. S1). In all the studies indicated below, the liposomes were freshly prepared, characterized, and used within 5 days post preparation to ensure stability and consistency.

Drug Photorelease From LBC

Although PSs can be released from liposomes through lysosomal degradation and other internalization processes, these cellular release mechanisms are slow processes and unable to completely and simultaneously release drugs from liposomes (26). Therefore, we investigated whether BPD in the bilayer can be activated to damage the lipid film and enhance drug release from liposomes, that is, light-activated drug release. We induced PSs release from LBC, and the results are presented in Figure 3b. There was minimal release of BPD (23.3%) and Cy5-927 (22.3%) under dark conditions (no irradiation with laser) at 37°C in 10% fetal bovine serum. As positive controls, LBC were dissolved in DMSO to disrupt liposomes and enable drug release. This process yielded 87.9% and 85.9% release of BPD and Cy5-927, respectively. Meanwhile, 84.8% and 83.4% release were observed for BPD and Cy5-927, respectively, under 10 J/cm^2 690 nm laser irradiation; these values were not significantly different from those in the positive group (dissolved in DMSO). By comparing the release percentages following irradiation with 690 nm laser and dissolvement in DMSO, we concluded that BPD (encapsulated in

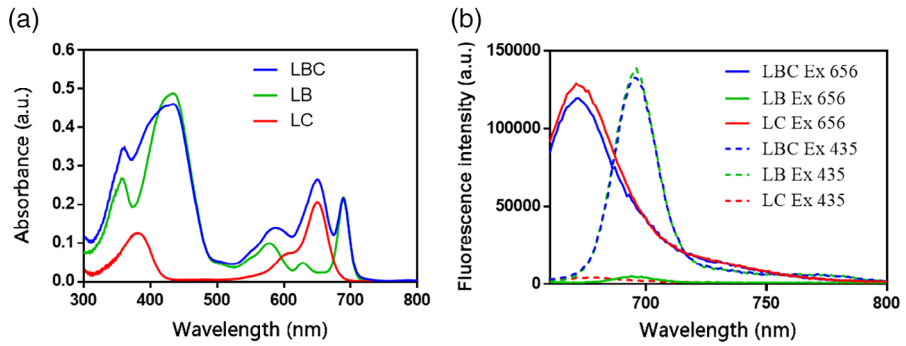

Figure 2. (**a**) Absorption spectra of BPD in NL (LB), Cy5-927 in NL (LC), and NL-co-encapsulated BPD and Cy5-927 (LBC). (**b**) Fluorescence spectra of LB, LC and LBC. Ex = 435 nm and Ex = 656 nm. [Color figure can be viewed at wileyonlinelibrary.com]

the bilayer) exhibited very good photorelease ability to release drugs from LBC.

STORM Imaging of LBC

A small droplet of LBC was placed on a coverslip to induce photo blinking under laser irradiation at 656 nm. The blinking data were recorded by using a home-built super-resolution imaging system. Although super-resolution localization microscopy is a powerful tool for studying nanoscale biological structures, its time-consuming data acquisition has hindered its application in live-cell imaging. A recently developed variation of localization microscopy, Bayesian analysis of blinking and bleaching (3B), provides the possibility of observing cellular dynamics below the diffraction limit (27). The 3B analysis provides the possibility of observing cellular dynamics below the diffraction limit (27). By using a hidden Markov model (HMM), 3B analysis allows overlapping multiemitter localization from data that would be impossible to analyze with standard single-molecule localization algorithms. In exchange for rapid data acquisition, 3B requires a long analysis time to solve the HMM model for molecular localization. The 3B algorithm can be manipulated in the standard way as Java plugin in ImageJ images and offers the possibility of observing cell dynamics at super-resolution (28). In our research, the blinking data for super-resolution imaging were analyzed by using the ImageJ plugin open-source package for 3B analysis software, which includes both 3B analysis and super-resolution image reconstruction.

As shown in Figure 4, the 3B super-resolution images showed significant improvement in spatial resolution, compared with the wide-field images. The ring structure peculiar to nanoliposomes was clearly recognizable, as shown in Figure 4b. More interestingly, piles of several nanoliposomes can still be clearly identified, as shown in Figure 4d.

The *In Vitro* Efficiency of LBC for PDT

To evaluate the *in vitro* efficacy of LBC for PDT, HeLa cells were incubated for 90 min with different reagents prior to PDT irradiation. Cell viability was analyzed for 24 h post-treatment using the CCK-8 test. As shown in Figure 5, no dark toxicity was observed in HeLa cells incubated with free BPD (B), LB, and LBC. No cell death was observed in the light control group (10 J/cm^2 laser irradiation). Under 690 nm laser irradiation, the cells treated with BPD, LB, and LBC showed viabilities of 0.294, 0.269, and 0.248, respectively. Although these three groups showed significantly higher phototoxicity than that of the other groups, cell viabilities in the BPD, LB, and LBC groups were not significantly different, thus indicating that the in vitro efficacy of BPD, LB, and LBC for PDT were similar.

Discussion

In this study, we presented a co-delivery strategy of BPD and Cy5-927 to tumor cells for effective PDT. Co-encapsulation of BPD and Cy5-927 in LBC allows both simultaneous delivery of

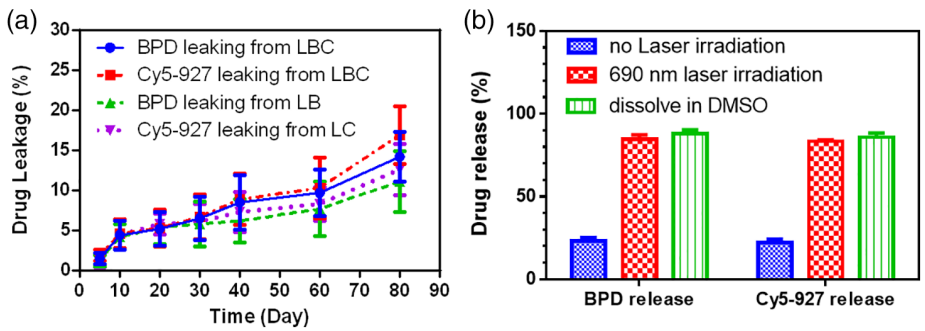

Figure 3. (**a**) Monitoring the leakage of BPD and Cy5-927 from BPD in NL (LB), Cy5-927 in NL (LC) and NLco-encapsulated BPD and Cy5-927 (LBC) stored at 4°C for over 2 months. (**b**) BPD and Cy5-927 release from LBC under dark conditions (no laser irradiation), 10 J/cm2 690 nm laser irradiation and dissolving in DMSO. [Color figure can be viewed at wileyonlinelibrary.com]

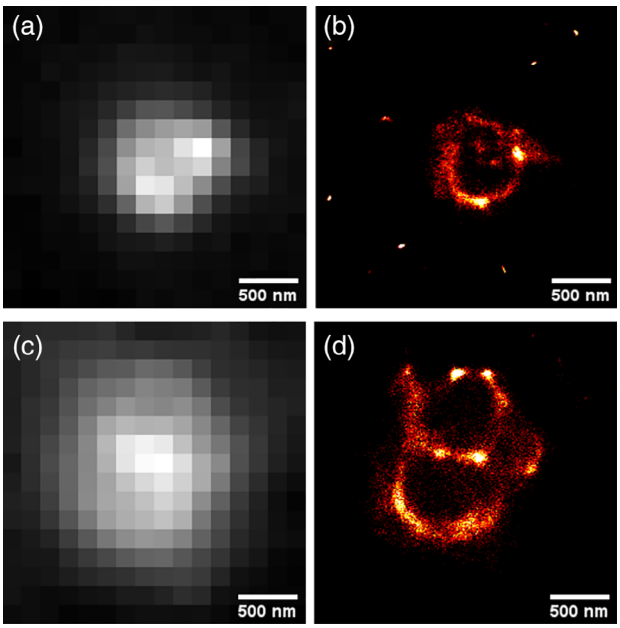

Figure 4. Super-resolution imaging of NL-co-encapsulated BPD and Cy5-927 (LBC). (**a**) and (**c**) wide-field images. (**b**) and (**d**) Bayesian analysis of the blinking and bleaching (3B analysis) results. [Color figure can be viewed at wileyonlinelibrary.com]

these drugs to a region of interest and observation of the fine nanostructures of liposomes and active PDT. The size of the fabricated liposome is around 200 nm, which is appropriate size for enhanced permeation through the leaky vasculature (13). Cholesterol was added to the liposome formulation to modulate membrane permeability and biological stability, DOTAP were added in lipid film to get the cationic liposome with positive potential to enhance the stability and drug delivery (29). Furthermore, PEG-2000 has been added to the lipid film to form

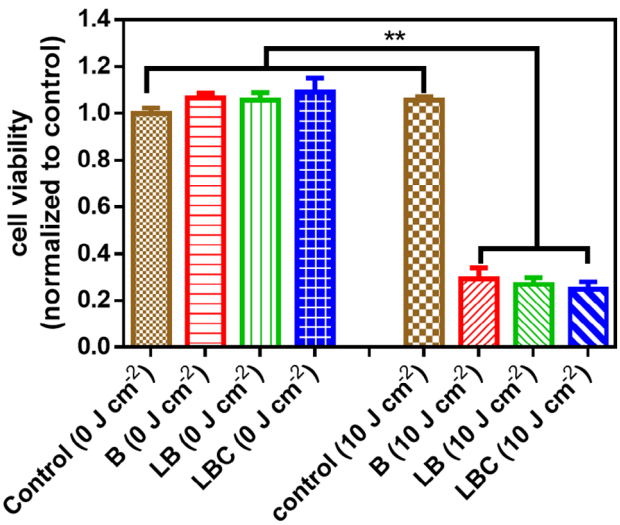

Figure 5. HeLa cells survival 1 day post-PDT. Free BPD (B), BPD in NL (LB) and NL-co-encapsulated BPD and Cy5-927 (LBC) all contained 250 nM BPD. Statistical significance was calculated by t-test: ** $P < 0.01$. [Color figure can be viewed at wileyonlinelibrary.com]

the poly(ethyleneglycol)-modified liposomes (PEGylated liposomes). PEGylation strategy is able to alter biodistribution, prolong circulation half-life, and avoid the recognition and subsequent uptake by the reticuloendothelial system (RES) (30).

The absorbance spectrum of LB has shown that BPD has a strong absorbance peak at 689 nm. Therefore, 690 nm laser was chosen for PDT in our research. This wavelength is in the therapeutic window and has deep penetration in tissue. The maximum absorbance peak of LC is 662 nm; therefore, 656 nm laser was chosen to excite Cy5-927 for STORM imaging. The fluorescence spectrum of LB has shown that the fluorescence intensity of BPD was very low at 656 nm excitation. So BPD has less influence on the fluorescence signal in LBC super-resolution optical imaging. Visualization of liposomes in PDT is one of the aims of our research. The STORM imaging results showed that LBC can be identified, and the lipid layer of LBC can also be visualized. This result indicated that our co-encapsulation strategy was feasible for application in PDT. In future research, we will improve the STORM imaging method for smaller-sized liposomes. Overall, our current research suggested that LBC can be utilized in super-resolution optical imaging and that BPD had low effect on the imaging results.

In addition, the effect of Cy5-927 on the drug photorelease and PDT efficiency of BPD in LBC was investigated. Spatial and temporal light-triggered drug photorelease enabled specific delivery of the drugs to target cells while reducing overall systemic toxicity (31). In our study, BPD encapsulated in the lipid bilayer enhanced the release of both BPD and Cy5-927 (Fig. 3b). For comparison, Peng et al. co-encapsulated the chemotherapy agent doxorubicin and the PSs chlorin e6 in liposomes (PL-Dox-Ce6), in which chlorin e6 was used to trigger doxorubicin release. This previous study highlighted that the combined regimen of PDT and chemotherapy showed higher efficacy than either therapy alone (32). Moreover, a recent study by Spring et al. introduced liposomes with photoactivable multi-inhibitor nanoliposome (PMIL) doped with BPD in the lipid bilayer and encapsulated cabozantinib (XL184), a multikinase inhibitor, inside the nanoliposomes. By spatiotemporally controlled drug release, the PMIL was shown to reduce systemic drug exposure and associated toxicities for cancer therapy (12). In our study, co-encapsulation of BPD and Cy5-927 in LBC had similar function as PL-Dox-Ce6 and PMIL. Under 690 nm laser exposure, activated BPD can lead to damage in the PEGylated lipid bilayer and, ultimately, release of BPD and Cy5-927. In future research, we will investigate changes in the fine structure of LBC in the photorelease process by using STORM imaging, which will reveal more details on changes in the lipid layers under photosensitive reaction.

In our research, the *in vitro* effects of free BPD, LB, and LBC for PDT were shown to have no significant difference. It should be noted that free BPD was initially dissolved in DMSO owing to its hydrophobic characters. Although the concentration of DMSO was very low, it is still toxic to cells. In contrast, LB and LBC were dissolved in PBS, which has virtually no toxicity to cells. In addition, nanoliposome has higher *in vivo* tumor targeting and retention abilities, beneficial for imaging and monitoring of PDT. The similar effects of LB and LBC for PDT indicated that Cy5-927 had low influence on the efficiency of BPD for PDT.

Therefore, the PDT process can be investigated by using LBC and super-resolution optical imaging. Furthermore, Cy5-927 contained a biomolecular target that can target VDPs in the mitochondria to visualize ultra-fine mitochondrial structures. In future research, LBC-containing HeLa cells will be used to investigate the intracellular localization and cellular PDT process of LBC by using both fluorescence and STORM imaging. Co-encapsulation of photoswitchable probes and PSs was shown to be a new feasible method for further investigation of liposome application in PDT.

Conclusions

To improve the efficiency of PSs for PDT, liposomes are presently used as one of the most optimal carriers for PDT. It is important to investigate the function of liposomes in the photosensitive process to optimize liposome-based PDT. In our research, co-encapsulation of BPD and Cy5-927 in LBC was performed to observe the liposome on nanoscale. Our results showed that LBC could be visualized by super-resolution imaging. In addition, the efficiency of BPD for PDT was not decreased following co-encapsulation with Cy5-927 in LBC. Thus, these liposomes can be used as an optimal carrier to investigate liposome-based PDT, which will promote our understanding of the PDT process at the micro level, providing guidance to optimize PDT trails.

Acknowledgments

This work has been partially supported by the National Natural Science Foundation of China (61705139/61875135/61525503/61620106016/61835009/81727804), (Key) Project of Department of Education of Guangdong Province(2015KGJHZ002/2016KCXTD007), Guangdong Natural Science Foundation Innovation Team (2014A030312008, 2017A030310136), Shenzhen Basic Research Project (JCYJ20150930104948169, JCYJ20160328144746940, JCYJ20170412105003520, JCYJ20170818090620324), China and Postdoctoral Science Foundation (2017 M612724), China.

Conflict of interest

The authors have declared that no competing interest exists.

Literature Cited

1. Hasan T, Ortel B, Moor ACE, Pogue BW. Photodynamic therapy of cancer. In: Kufe DW, Pollock RE, Weichselbaum RR, Robert C, Bast J, Gansler TS, Holland JF, Emil Frei I, editors. Holland-Frei Cancer Med. . 6th ed. Hamilton, Canada: B.C. Decker, 2003; p. 605–622.
2. Ježek P, Nekvasil M, Škobisová E, Urbánková E, Jirsa M, Zadinová M, Poučková P, Klepáček I. Experimental photodynamic therapy with meso-tetrakisphenylporphyrin (TPP) in liposomes leads to disintegration of human amelanotic melanoma implanted to nude mice. Int J Cancer 2003;103:693–702.
3. Huang H, Hasan T. The "Nano" world in photodynamic therapy. Austin J Nanomedicine Nanotechnol 2014;2:1–4.
4. Lucky SS, Soo KC, Zhang Y. Nanoparticles in photodynamic therapy. Chem Rev 2015;115:1990–2042.
5. Obaid G, Broekgaarden M, Bulin A, Huang H, Kuriakose J, Hasan T. Photonanomedicine: A convergence of photodynamic therapy and nanotechnology. Nanoscale 2016;8:12471–12503.
6. Huggett MT, Jermyn M, Gillams A, Illing R, Mosse S, Novelli M, Kent E, Bown SG, Hasan T, Pogue BW, et al. Phase I/II study of verteporfin photodynamic therapy in locally advanced pancreatic cancer. Br J Cancer 2014;110:1698–1704.
7. Lancet JE, Cortes JE, Hogge DE, Tallman MS, Kovacsovics TJ, Damon LE, Komrokji R, Solomon SR, Kolitz JE, Cooper M, et al. Phase 2 trial of CPX-351, a fixed 5:1 molar ratio of cytarabine/daunorubicin, vs cytarabine/daunorubicin in older adults with untreated AML. Blood 2014;123:3239–3246.
8. Huang HC, Mallidi S, Liu J, Te CC, Mai Z, Goldschmidt R, Ebrahim-Zadeh N, Rizvi I, Hasan T. Photodynamic therapy synergizes with irinotecan to overcome compensatory mechanisms and improve treatment outcomes in pancreatic cancer. Cancer Res 2016;76:1066–1077.
9. Tangutoori S, Spring BQ, Mai Z, Palanisami A, Mensah LB, Hasan T. Simultaneous delivery of cytotoxic and biologic therapeutics using nanophotoactivatable liposomes enhances treatment efficacy in a mouse model of pancreatic cancer. Nanomedicine 2016;12:223–234.
10. Morton SW, Lee MJ, Deng ZJ, Dreaden EC, Siouve E, Shopsowitz KE, Shah NJ, Yaffe MB, Hammond PT. A nanoparticle-based combination chemotherapy delivery system for enhanced tumor killing by dynamic rewiring of signaling pathways. Sci Signal 2014;7:ra44.
11. He C, Liu D, Lin W. Self-assembled Core a Shell nanoparticles for combined chemotherapy and photodynamic therapy of resistant head and neck cancers. ACS Nano 2015;9:991–1003.
12. Spring BQ, Bryan Sears R, Zheng LZ, Mai Z, Watanabe R, Sherwood ME, Schoenfeld DA, Pogue BW, Pereira SP, Villa E, et al. A photoactivable multi-inhibitor nanoliposome for tumour control and simultaneous inhibition of treatment escape pathways. Nat Nanotechnol 2016;11:378–387.
13. Derycke ASL, de Witte PAM. Liposomes for photodynamic therapy. Adv Drug Deliv Rev 2004;56:17–30.
14. Kobayashi H, Watanabe R, Choyke PL. Improving conventional enhanced permeability and retention (EPR) effects; what is the appropriate target? Theranostics 2014;4:81–89.
15. Lo Y, Tsai J, Kuo J. Liposomes and disaccharides as carriers in spray-dried powder formulations of superoxide dismutase. J Control Release 2004;94:259–272.
16. Liu JX, Xin B, Li C, Xie NH, Gong WL, Huang ZL, Zhu MQ. PEGylated Perylenemonoimide-Dithienylethene for super-resolution imaging of liposomes. ACS Appl Mater Interfaces 2017;9:10338–10343.
17. Mishra A, Behera RK, Behera PK, Mishra BK, Behera GB. Cyanines during the 1990s: A review. Chem Rev 2000;100:1973–2012.
18. Guo Z, Park S, Yoon J, Shin I. Recent progress in the development of near-infrared fluorescent probes for bioimaging applications. Chem Soc Rev 2014;43:16–29.
19. Sun W, Guo S, Hu C, Fan J, Peng X. Recent development of Chemosensors based on cyanine platforms. Chem Rev 2016;116:7768–7817.
20. Rust MJ, Bates M, Zhuang X. Sub-diffraction-limit imaging by stochastic optical reconstruction microscopy (STORM). Nat Methods 2006;3:793–795.
21. Dempsey GT, Vaughan JC, Chen KH, Bates M, Zhuang X. Evaluation of fluorophores for optimal performance in localization-based super-resolution imaging. Nat Methods 2011;8:1027–1036.
22. Samanta S, Gong W, Li W, Sharma A, Shim I, Zhang W, Das P, Pan W, Liu L, Yang Z, et al. Organic fluorescent probes for stochastic optical reconstruction microscopy (STORM): Recent highlights and future possibilities. Coord Chem Rev 2019;380:17–34.
23. Shen S, Li X, Cullen WR, Weinfeld M, Le XC. Arsenic binding to proteins. Chem Rev 2013;113:7769–7792.
24. Tominaga H, Ishiyama M, Ohseto F, Sasamoto K, Hamamoto T, Suzuki K, Watanabe M. A water-soluble tetrazolium salt useful for colorimetric cell viability assay. Anal Commun 1999;36:47–50.
25. Postigo F, Mora M, De Madariaga MA, Nonell S, Sagristá ML. Incorporation of hydrophobic porphyrins into liposomes: Characterization and structural requirements. Int J Pharm 2004;278:239–254.
26. Gerasimov OV, Boomer JA, Qualls MM, Thompson DH. Cytosolic drug delivery using pH- and light-sensitive liposomes. Adv Drug Deliv Rev 1999;38:317–338.
27. Cox S, Rosten E, Monypenny J, Jovanovic-talisman T, Burnette DT, Lippincott-schwartz J, Jones GE, Heintzmann R. Bayesian localization microscopy reveals nanoscale podosome dynamics. Nat Methods 2012;9:195–200.
28. Rosten E, Jones GE, Cox S. ImageJ plug-in for Bayesian analysis of blinking and bleaching. Nat Methods 2013;10:98–99.
29. Campbell RB, Balasubramanian SV, Straubinger RM. Phospholipid-cationic lipid interactions: Influences on membrane and vesicle properties. Biochim Biophys Acta 2001;1512:27–39.
30. Oliveira MF, Guimarães PPG, Gomes ADM, Suárez D, Sinisterra RD. Strategies to target tumors using nanodelivery systems based on biodegradable polymers, aspects of intellectual property, and market. J Chem Biol 2013;6:7–23.
31. Pattni BS, Chupin VV, Torchilin VP. New developments in liposomal drug delivery. Chem Rev 2015;115:10938–10966.
32. Peng P-C, Hong R-L, Tsai Y-J, Li P-T, Tsai T, Chen C-T. Dual-effect liposomes encapsulated with doxorubicin and chlorin e6 augment the therapeutic effect of tumor treatment. Lasers Surg Med 2015;1:1–11.